JLab PAC12 Proposal Cover Sheet

This document must be received by close of business on June 26, 1997

Jefferson Lab
User Liaison Office, Mail Stop 12 B
12000 Jefferson Avenue
Newport News, VA 23606

(Choose one)

☒ New Proposal Title: Correlated spectral function and (e,e'p) reaction mechanism

☐ Update Experiment Number:

☐ Letter-of-Intent Title:

Contact Person

Name: Ingo Sick
Institution: Institut für Physik, Universität Basel
Address: Klingelbergstrasse 82
Address: CH-4056 BASEL, Switzerland
City, State, ZIP/Country:
Phone: ++4161 2673741 Fax: ++4161 2673748
E-Mail: SICK@UBACLU.UNIBAS.CH

Experimental Hall: C Days Requested for Approval: 15

Jefferson Lab Use Only

Receipt Date: 6/26/97 97-006

By:

LAB RESOURCES LIST

JLab Proposal No.: _____ Date _____
(For JLab ULO use only.)

List below significant resources — both equipment and human — that you are requesting from Jefferson Lab in support of mounting and executing the proposed experiment. Do not include items that will be routinely supplied to all running experiments such as the base equipment for the hall and technical support for routine operation, installation, and maintenance.

Major Installations *(either your equip. or new equip. requested from JLab)*

_____

_____

_____

_____

_____

New Support Structures: _____

_____

_____

_____

Data Acquisition/Reduction

Computing Resources: _____

_____

_____

_____

New Software: _____

_____

_____

_____

Major Equipment

Magnets: _____

_____

Power Supplies: _____

_____

Targets: _____

_____

Detectors: _____

_____

Electronics: _____

_____

Computer Hardware: _____

_____

Other: _____

_____

Other: _____

_____

_____

_____

HAZARD IDENTIFICATION CHECKLIST

JLab Proposal No.: _____ Date: _____
(For CEBAF User Liaison Office use only)

Check all items for which there is an anticipated need.

Cryogenics
- _____ beamline magnets
- _____ analysis magnets
- X target
  - type: LH_2
  - flow rate: Hall C
  - capacity: _____

Electrical Equipment
- _____ cryo/electrical devices
- _____ capacitor banks
- _____ high voltage
- _____ exposed equipment

Radioactive/Hazardous Materials
List any radioactive or hazadorous/ toxic materials planned for use:
_____
_____
_____
_____

Pressure Vessels
- _____ inside diameter
- _____ operating pressure
- _____ window material
- _____ window thickness

Flammable Gas or Liquids
- type: _____
- flow rate: _____
- capacity: _____

Drift Chambers
- type: _____
- flow rate: _____
- capacity: _____

Other Target Materials
- ___ Beryllium (Be)
- ___ Lithium (Li)
- ___ Mercury (Hg)
- ___ Lead (Pb)
- ___ Tungsten (W)
- ___ Uranium (U)
- ___ Other (list below)

_____
_____

Vacuum Vessels
- _____ inside diameter
- _____ operating pressure
- _____ window material
- _____ window thickness

Radioactive Sources
- _____ permanent installation
- _____ temporary use
- type: _____
- strength: _____

Large Mech. Structure/System
- _____ lifting devices
- _____ motion controllers
- _____ scaffolding or
- _____ elevated platforms

Lasers
- type: _____
- wattage: _____
- class: _____

Installation:
- _____ permanent
- _____ temporary

Use:
- _____ calibration
- _____ alignment

Hazardous Materials
- ____ cyanide plating materials
- ____ scintillation oil (from)
- ____ PCBs
- ____ methane
- ____ TMAE
- ____ TEA
- ____ photographic developers
- ____ other (list below)

_____
_____

General:

Experiment Class:
- X Base Equipment
- _____ Temp. Mod. to Base Equip.
- _____ Permanent Mod. to Base Equipment
- _____ Major New Apparatus

Other: _____
_____

BEAM REQUIREMENTS LIST

JLab Proposal No.: _____ Date: _____

Hall: C Anticipated Run Date: _____ PAC Approved Days: _____

Spokesperson: Ingo Sick Hall Liaison: _____
Phone: ++ 41 61 267 3741
E-mail: SICK@UBACLU.UNIBAS.CH

List all combinations of anticipated targets and beam conditions required to execute the experiment. (This list will form the primary basis for the Radiation Safety Assesment Document (RSAD) calculations that must be performed for each experiment.)

Condition No.	Beam Energy (MeV)	Mean Beam Current (μA)	Polarization and Other Special Requirements (e.g., time structure)	Target Material (use multiple rows for complex targets — e.g., w/windows)	Material Thickness (mg/cm²)	Est. Beam-On Time for Cond. No. (hours)
1	4000	100	cw, non-pol.	^{12}C,H_2O,^{27}Al /^{56}Fe,^{197}Au	1000/500	140
2	3200	20	"	"	"	80
3	3200	100	"	"	"	42
4	3200	100	"	"	"	9
5	2400	100	"	"	"	14
6	4000	100	"	LH_2	Hall C LH_2	6
7	3200	20	"	"	"	6
8	3200	100	"	"	"	6
9	3200	100	"	"	"	6
10	2400	100	"	"	"	6
(11)	(2800)	100	"	^{12}C / ^{197}Au	1000/500	15

The beam energies, E_{Beam}, available are: $E_{Beam} = N \times E_{Linac}$ where N = 1, 2, 3, 4, or 5. E_{Linac} = 800 MeV, i.e., available E_{Beam} are 800, 1600, 2400, 3200, and 4000 MeV. Other energies should be arranged with the Hall Leader before listing.

TJNAF Proposal

Correlated spectral function and (e,e'p) reaction mechanism

A. Honegger, J. Jourdan, M. Mühlbauer, Th. Petitjean, I. Sick, G. Warren, J. Zhao
Departement für Physik und Astronomie,
Universität Basel, Basel, Schweiz

S. Bueltmann, Z. Cheng, D. Crabb, D. Day, J. McCarthy,
D. McNulty, Y. Prok, O. Rondon, B. Zihlmann
Dept. of Physics, Univ. of Virginia,
Charlottesville, VA

O. Benhar
Istituto Superiore di Sanita and INFN,
Roma, Italy

R. Ent, D. Mack, J. Mitchell
TJNAF

June 24, 1997

Abstract

We propose an (e,e'p) experiment to measure the strength of the spectral function $S(k, E)$ at large values of k and E resulting from short-range nucleon-nucleon correlations. A study of previous (e,e'p) experiments shows that much of the available data is dominated by two-step processes. We identify the kinematics that could give access to the strength at large k, E without unacceptably large corrections due to multistep-processes, and propose a corresponding experiment. This experiment at the same time is designed to also provide data in the region where multi-step processes are expected to dominate, such as to allow a check of the theoretical calculations we are performing.

1 Introduction

From experimental data on (e,e'p) we have gained considerable knowledge on the single-particle structure of nuclei. These measurements, performed at energies $\leq$600 MeV in the past, have yielded the removal energies, momentum distributions and spectroscopic factors of many single-particle states.

Detailed analysis of these data also have provided us with integral quantities such as occupation numbers. The most accurate occupation number comes from the CERES analysis of (e,e), (e,e'p) and transfer-data on nuclei in the Pb-region (for a review see [1]). They show that in nuclei the single-particle states near the Fermi edge are occupied to $\sim$ 75% only. Much of this depopulation occurs due to the short-range correlations. The strong short-range repulsion of the N-N interaction scatters nucleons to states of higher momentum k and high removal energy E, and this strength is not visible when studying the single-particle properties at low k, E.

Microscopic calculations of the nuclear spectral function — feasible for ^{3}He [2, 3, 4] and infinite nuclear matter [5] — show that this correlated strength occurs at large k *and* large E, where k and E are related by $E \sim k^2/2m_N$. This is easily understandable: Short-range 2N collisions scatter the two nucleons into states with momentum $\vec{k}$ and $-\vec{k}$ ($k \gg k_F$). When knocking out, via (e,e'p), one nucleon with momentum $\vec{k}$, the other nucleon, lacking its correlated partner, will also leave the nucleus, with momentum $-\vec{k}$. The energy it costs to put this nucleon onto the mass shell, $\sim (-\vec{k})^2/2m_N$, also has to be provided by the electron, and appears in (e,e'p) as a large missing energy $E \sim (-\vec{k})^2/2m_N$.

A number of (e,e'p) experiments addressing the region of large k, large E have already been carried out. These experiments give a very contradictory impression on the processes that take place. Some experiments, particularly the series performed at Bates, seem to find at large E a huge excess of strength, which is claimed to be due to multi-body currents (two-body currents are said to be not enough). Other data, in particular the ones for light nuclei coming from Saclay and Mainz, seem to find values for the spectral function that are more or less in line with expectation.

In this proposal, we use the existing data to analyze the origin of the problem. We then propose a new experiment that avoids these difficulties as far as possible.

2 Spectral function

The spectral function $S(k, E)$ describes the probability to find in the nucleus a proton of initial momentum $\vec{k}$ and removal energy E. Integration of $S(k, E)$ over E gives the

nucleon momentum distribution $n(k)$.

For the A=3 system the wave function can be calculated by solving the Schrödinger (Faddeev) equation for 3 nucleons interacting via one of the standard N-N interactions [2, 3, 4]. For infinite nuclear matter, the spectral function can be calculated from the wave function derived using correlated basis function theory (CBF) [5]. For nuclei with $3 < A < \infty$ approximate treatments are required.

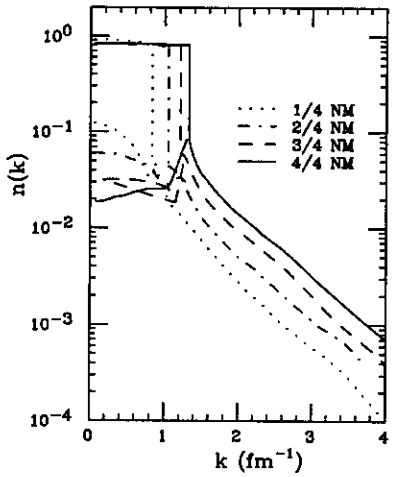

Figure 1: Nuclear matter momentum distributions for various nuclear matter densities (fractions of density of the experimental NM density). The lower lines for $k < k_F$, and the lines for $k > k_F$ correspond to the correlated part.

In ref. [6, 7] the spectral function of *nuclear matter* of various saturation densities has been split into the single-particle and the correlated parts. For finite nuclei the correlated part can be calculated using the local density approximation (LDA); for short-range properties the LDA is expected to be an excellent approximation. The single-particle part of the spectral function can be calculated using realistic single-particle models, or can be parameterized using the wave functions fitted to (e,e'p) data at low k, E. Tests for ^{16}O and ^{4}He have shown [7] that this spectral function calculated in LDA does extremely well in reproducing exact results for $n(k)$.

In fig. 1 we give the split of $n(k)$ for nuclear matter into the correlated and single-particle parts, fig. 2 gives the corresponding strength as a function of E.

In fig.3 we show a contour plot of the strength of $S(k, E)$. At $k < k_F, E < 80$MeV the strength is dominated by the single-particle properties, at large k, E one recognizes the ridge $E \sim k^2/2m_N$ due to short-range N-N correlations. The total amount of strength in this ridge amounts to $\sim 20\%$ of Z. This strength is spread over a large range in k, E, however, which makes $S(k, E)$ small, hence difficult to measure.

The strength of $S(k, E)$ is distributed roughly symmetrically relative to the ridge $E \simeq k^2/2M$. This is easily understood: while the relative momentum $2\vec{k}$ of the two nucleons

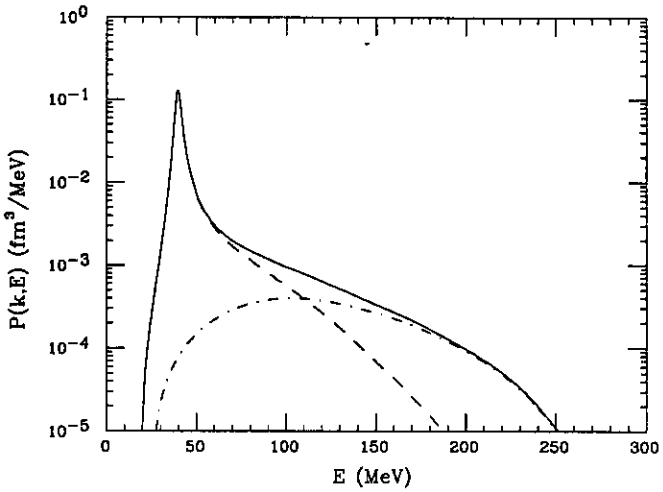

Figure 2: Nuclear matter spectral function at a fixed nucleon momentum $k/k_F = 0.75$. The dashed (dotdashed) curves give the uncorrelated (correlated) parts.

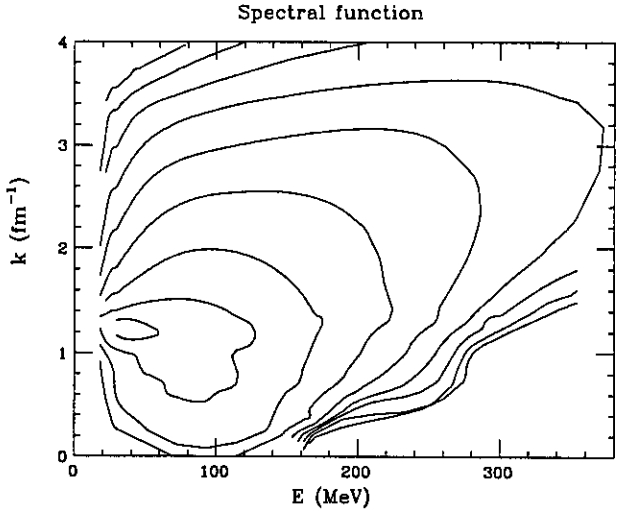

Figure 3: Contour plot of the logarithm of the Oxygen spectral function $S(k, E)$

gives rise to the ridge (which is a line $E = k^2/2M$ for the deuteron), the movement of the center-of-mass of the two-nucleon pair relative to the CM of the nucleus gives the width. This is demonstrated directly in the model-spectral function constructed by Ciofi *et al*[8]. The two sides of the ridge thus contain the *same physics*, which then can be accessed by looking at one side or the other, depending on additional considerations. The main information on 2-nucleon correlations is found in the overall amplitude of $S(k, E)$ in the

region of the top of the ridge. Or, expressed in terms of $n(k)$, it is contained in the overall amplitude of the momentum distribution for momenta k significantly larger than k_F.

Several pieces of experimental information support this picture. The inclusive (e,e') cross section at large momentum transfer $\vec{q}$ and values of the Bjorken scaling variable x between 1.5 and 2 has been shown to be sensitive to the strength of the spectral function $S(k,E)$ at large k,E [9]. The experimental cross sections are explained quantitatively when using microscopic spectral functions with the properties described above. Recent experiments on (e,e'p) at large k, but *low* E [10, 11] also have shown that the strength of the spectral function in this region is very small; this is *not* the region to look for short range correlations. The (e,e'p) experiments on ^{4}He and ^{3}He [12, 13] show, for still relatively low k,E, the beginning of the "ridge" of the spectral function at $E \sim k^2/2m_N$.

3 Multi-step reactions

The determination of the correlated strength involves a measurement of the spectral function at large initial (missing) momentum k and large removal (missing) energy E. This can be done only to the extent that multi-step reactions do not simulate such strength.

The importance of multi-step reactions is already known from past studies of (e,e'n) at low k,E where $S(k,E)$ is large [14]. (e,e'n) cannot be understood in terms of PWIA or DWIA alone; (e,e'p) followed by a (p,n) charge exchange reaction simulates (e,e'n). This two-step process is important as the (e,e'p) cross section is significantly larger than the PWIA (e,e'n) cross section. In this case the two-step process becomes important even though the ratio between (e,e'p) and (e,e'n) is not *very* large, it typically amounts to a factor of $5 \div 10$ only. This fact immediately indicates that it will be difficult to address the strength of the spectral function at large k,E, as this strength is typically 5 times smaller than the one at low k,E, and moreover spread thinly over a very large region.

From (e,e'p) experiments at low k,E we know that experimentally one detects only a fraction of the strength expected in PWIA. The proton on its way out of the nucleus interacts, and gets "absorbed". This process in the standard DWIA analysis of the data is accounted for using a complex optical potential. The imaginary part leads to a reduction of the proton flux that amounts to 30% for light nuclei, rising to 70% for heavy nuclei.

When interested in (e,e'p) to single-particle states one is only dealing with this final state interaction (FSI) in terms of protons that "disappear" from the channel of interest. These protons, of course, do not "disappear". They typically, at the energies relevant to studies of large k,E, undergo (p,pN) processes, *i.e.* scatter quasielastically off another, initially bound, nucleon N. They loose enough energy and change enough their momentum to "disappear" from the (e,e'p) channel leading to discrete states of the recoil nucleus. These protons, however, all "reappear" in the region relevant to studies of large missing energy and missing momentum! The (e,e'p) process on a proton of low k',E', followed by (p,p'N), simulates (e,e'p) with the energy and momentum of the nucleon N' added to the k',E' of the primary proton (see fig.4,5).

For kinematics typical for studies of large k,E, — recoil proton energies of say 500

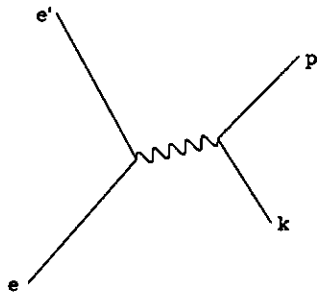

Figure 4: Single-step (e,e'p) process on nucleon with initial momentum k and removal energy E.

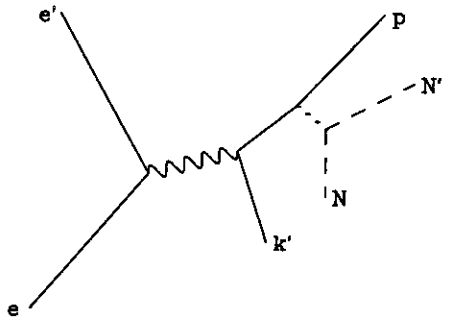

Figure 5: Two-step process involving knockout of a nucleon with initial momentum, k' and energy E', followed by (p,p'N) scattering process, leading to the same final electron and proton as (e,e'p) of figure 4.

MeV — the energy- and momentum loss in a (p,p'N) reaction is of order 100-200 MeV and 600 MeV/c respectively, as the p-N scattering angles on average are large (the p-N angular distribution is rather flat as function of scattering angle). The strength of (e,e'p) + (p,p'N) thus is spread over a range of k, E comparable to the one of interest for the study of short-range correlations (see figure 3).

The relative strength of these 2-step reactions compared to the one-step reaction is

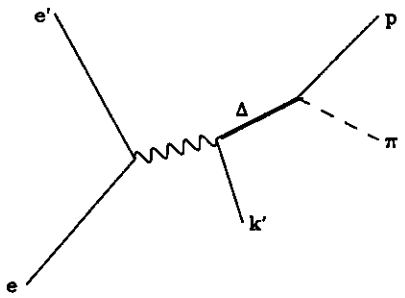

Figure 6: Two-step process involving knockout of nucleon with initial momentum k' and energy E' including excitation to N*, followed by N* $\rightarrow \pi$ + p, leading to same final electron and proton as (e,e'p) of figure 4.

large. As explained above, the correlated strength amounts to $\sim$ 20% of Z. 30–70% of (100% –20%) · Z of the strength is subject to (the dominating) (p,p'N) process which shifts strength to (apparent) large k, E. The ratio of noise to signal in the large k/large$E$ region thus is

$$\frac{(30 \div 70\%) \cdot 80\% \cdot Z}{20\% \cdot Z} = \frac{1.3 \div 3}{1} \qquad (1)$$

In the region of large k, E the "noise" due to (e,e'p) + (p,p'N) strength which is misinterpreted as (e,e'p) overwhelms the true correlated strength by a factor 1.3 – 3! In practice, the situation is even worse, as only part of the strength resulting from $S(k, E)$ at large k, E is observed; the corresponding final-state nucleons are also absorbed, a fact that increases the noise/signal ratio by another factor $1/(0.7 \div 0.3)$.

From these consideration it is clear that the complications due to the reaction mechanism are enormous indeed when trying to measure the true IA (e,e'p) strength at large k, E. One must consider this "noise" due to multistep reactions when trying to understand the data.

There is a second process which must be expected to play an important role: N(e,e'N*) followed by $N^* \rightarrow p + \pi$. This reaction, with N* = Δ, again can simulate (e,e'p), with the energy and momentum of the not-observed π being falsely interpreted as large initial E, k of the knocked-out proton. As the π is a light particle which has a high energy/momentum ratio, the problems here mainly concerns the region of large E.

One again can roughly estimate the strength that goes into this channel. For the momentum transfers relevant to studies of large k, E, the elastic e-N cross section is similar in magnitude to the one for Δ-excitation. For studies of the $E = 150 \div 200$ MeV

region, the tail of the Δ-resonance, which contains $\simeq$10% of the total strength, interferes with (e,e'p). This strength leads to a noise/signal ratio of

$$\frac{10\% \cdot Z}{20\% \cdot Z} \approx \frac{0.5}{1} \tag{2}$$

Here part of this strength may appear below π-production threshold if the decay of the excited N* leads to a bound state of the residual (A–1) nucleus (a process usually treated under the category of MEC rather than 2-step reactions involving the Δ). At the large q relevant for studies of large k, E the *incoherent* π-production on a single nucleon is likely to dominate over the process where the π would be reabsorbed by a second nucleon.

Although the noise/signal ratio due to Δ excitation is not as bad as the one due to (p,p'N), one still has to give serious considerations to this channel if one wants to suppress it to the point where one can determine the true single step (e,e'p) strength at large k, E.

From the above considerations it becomes clear that an understanding of data on (e,e'p) relevant for a study of $S(k, E)$ at large k, E vitally depends on the understanding of the contribution of multi-step reactions. A priori the noise due to these multi-step reactions is significantly bigger than the signal one is looking for.

The contributions of these multi-step reactions were largely ignored in the design of (e,e'p) experiments previously performed. Here, we use existing data to better understand where two-step reactions are indeed important.

4 Simulation of 2-step processes

4.1 Quasifree (p,p'N)

In this section we study potential contributions of 2-step processes to existing data. We emphasize the kinematics of the two-step processes of relevance to (e,e'p) — rather than the cross sections — as the kinematics alone are much more transparent. For kinematics that do suppress the unwanted processes as much as possible it then will pay to perform dynamical calculations; such calculations are under way.

At recoil proton energies of a few hundred MeV or higher, the energy range of interest for large k, E, the dominating final state interaction of protons is quasielastic scattering off other nucleons (figure 5). This process has straightforward kinematics and can easily be included.

The approach we have taken consists of the following. For various kinematics of past experiments relevant for studies of $S(k, E)$ at large k, E we have calculated all those kinematics which for an (e,e'p) + (p,p'N) two-step process gives the *same* scattered electron and recoil proton as the single-step (e,e'p) process of interest, i.e. we have calculated those 2-step processes which in an (e,e'px) experiment (with x not detected) are not distinguished from true (e,e'p).

Variables in this search are the momentum k' and the energy E' of the proton originally hit by the electron, and the scattering angle in the (p,p'N) process. We have, for simplicity,

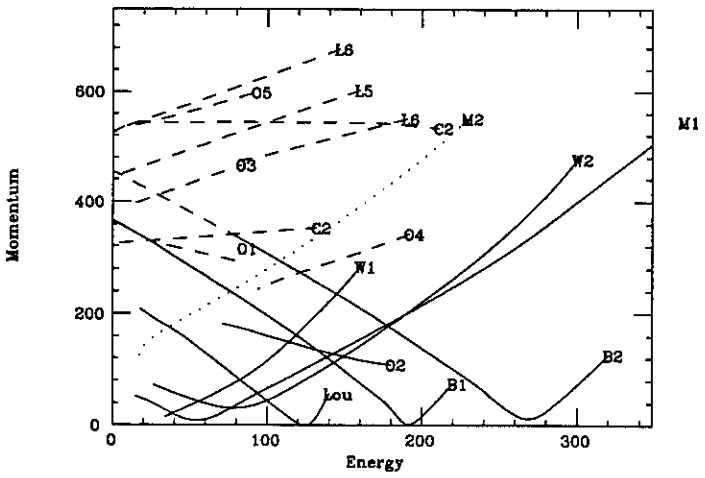

Figure 7: Kinematical coverage of existing (e,e'p) experiments of Lourie *et al* (Lou), Baghaei *et al* (B1,B2), Weinstein *et al* (W1,W2), Morrison *et al* (M1,M2), LeGoff *et al* (L1 – L6), Offerman *et al* (O1 – O6), Marchand *et al* (C1,C2). The solid (dashed) lines correspond to experiments with $\sigma_{exp} >> \sigma_{IA}$ ($\sigma_{exp} \simeq \sigma_{IA}$).

neglected the out-of-plane scattering in the (p,p'N) process, and we have neglected the fact that the second N before the secondary scattering did have a momentum of order k_F. These features both would lead to a *smearing* of the kinematics, but not to a *shift*.

The single-step cross section is given by the product of the spectral function $S(k, E)$ and the e-p cross section (times kinematical factors of order 1). The two-step cross section is given by the product of the spectral function $S(k', E')$ evaluated at a different k', E', the e-p cross section, the probability of the proton to do a (p,p'N) scattering on its way out of the nucleus, and the angle-dependent p-N scattering cross section. The latter two factors are largely independent of kinematics as the p-N cross section depends weakly on energy and angle. The main variable to consider thus is the value of $S(k', E')$, which, depending on the kinematics chosen, is the main factor influencing the signal/noise ratio.

The kinematics studied are those of existing (e,e'p) experiments [12, 15, 16, 17, 18, 19, 13, 20], and of (e,e'p) proposals [21, 22] aiming at large k, E. Figure 7 shows the region of the spectral function covered by the various experiments. Figure 8 shows, for one particular k, E, the range of k', E' that contributes to the (e,e'p) + (p,p'N) reaction; the running parameter is the p-N scattering angle. Figs.9 shows the same types of curves for other experiments.

Figs. 8-9 clearly show that for the kinematics of the Bates experiments [15, 16, 19, 18] the two-step (p,p'N) process contributes strength that originates from a region of the spectral function where $S(k', E')$ is *much larger* than the $S(k, E)$ one intends to measure using a single-step process. As the total strength contributed by (p,p'N) processes is

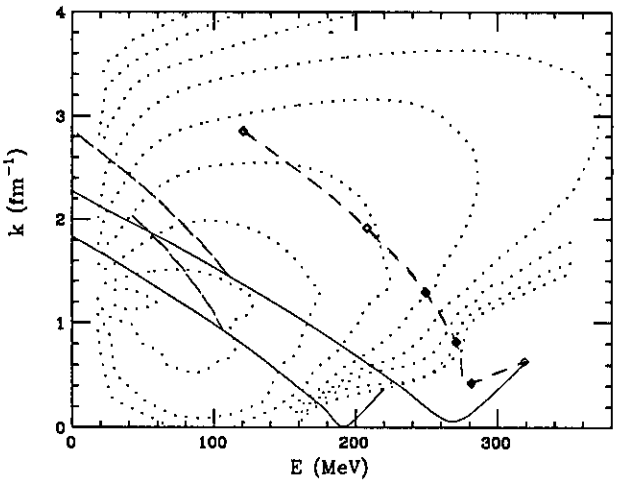

Figure 8: Kinematical coverage of $S(k, E)$ of Baghaei *et al* together with contour plot of $S(k, E)$. The dashed lines give the region of k', E' where the strength due to (e,e'p) followed by (p,p'N) comes from. The diamonds correspond to CM scattering angles of 0,20,40,60,.. degrees.

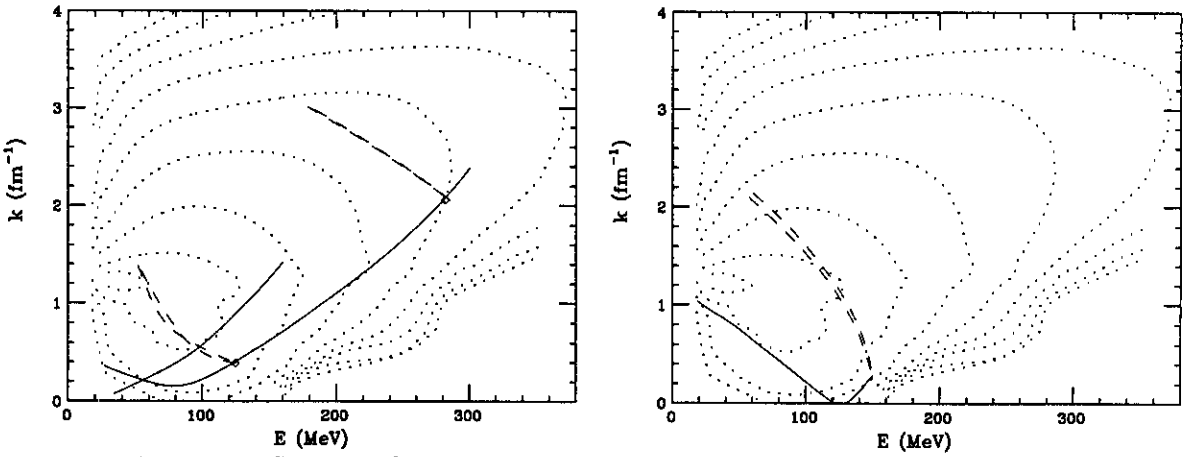

Figure 9: Same as figure 8, for experiment of Weinstein *et al* and Lourie *et al.*

large (see section 3), one must, in the region of k below the $E = k^2/2m$-ridge, expect to measure mainly two-step processes.

For the kinematics of the experiments performed at Saclay and Mainz [20, 12, 13] (see fig. 10), on the other hand, the region of the spectral function which contributes via (p,p'N) in general has a value of $S(k', E')$ which is *lower* than the $S(k, E)$ one intends to measure by single-step (e,e'p). As $S(k', E')$ falls off very quickly when going away from the

top of the ridge, one may hope that under these kinematical conditions the contributions of two-step processes become manageable and can be ultimately removed by theory.

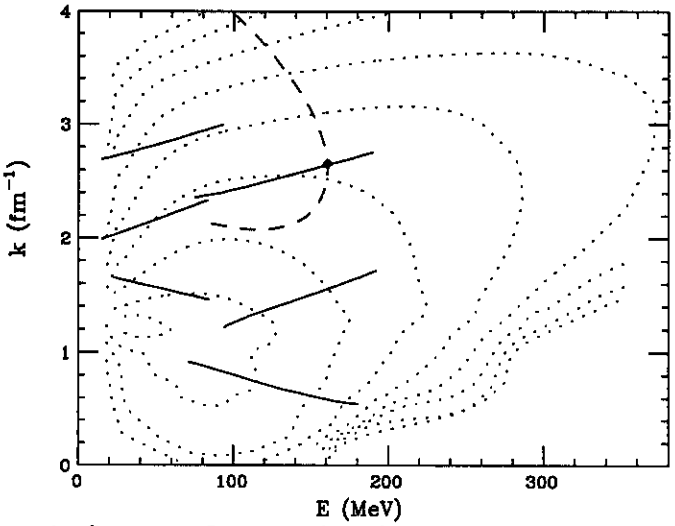

Figure 10: Same as figure 8, but for kinematics of Offerman *et al* (The (p,p'N) locus (dashed) is given for data set O6)

In order to understand better some of the published data, we have calculated for many of the experiments displayed in fig. 7 the impulse approximation (IA) (e,e'p) cross section, using the LDA spectral function and the SIGCC1 (e,e'p) cross section. These cross sections have been compared to the ones experimentally found. The interest of this comparison is not whether we can quantitatively explain the data (this would require a better $S(k,E)$, calculation of the standard FSI effects using optical potentials, radiative corrections of the data, etc.). The main question is: are the experimental cross sections within, say, a factor of two of the calculated ones in which case the reaction mechanism is close to IA and corrections can be handled, or are the experimental cross sections much larger than the ones calculated in which case multi-step reactions may dominate completely.

The results of these studies are coded in fig.7. Solid lines correspond to data where σ_{exp} is orders of magnitude larger than σ_{IA}, dashed lines correspond to data where $\sigma_{exp} \cong \sigma_{IA}$ (within the factor of two mentioned above). For the kinematics employed in the Bates experiments, the experimental cross section is orders of magnitude larger than calculated, for the Mainz/Saclay kinematics the two are close. The message of fig.7 is clear: there is a one to one correspondence between the value of σ_{exp}/σ_{IA} and the value of k', E' from which the strength contributing to (e,e'p) + (p,p'N) originates. If $S(k',E') \gg S(k,E)$ as is the case for k,E below the ridge, then $\sigma_{exp}/\sigma_{IA} \gg 1$, if $S(k',E') < S(k,E)$, then $\sigma_{exp}/\sigma_{IA} \sim 1$.

The considerations based on the kinematics of the two-step reactions thus allow to understand the empirical evidence in a variety of kinematics.

Figure 7 moreover shows some interesting detail. The data set of Baghaei *et al* corresponding to low E and large k, in the region up to the ridge of $S(k,E)$, receives contributions via two-step reactions from regions of *smaller* $S(k',E')$ only. In this region we find (contrary to statements made in the original publication, where no quantitative spectral function was available yet) that the cross section is close to the IA prediction.

We also point out that Takaki [23] has made numerical calculations of two-step processes. His calculation included the (p,p'N) process (but not the two-step process involving Δ-excitation, see below). His conclusion, for the kinematics of the data of Lourie *et al*, was that these (p,p'N) two-step process could not explain the large strength found at large missing energy. This led to the conclusion that many-body mechanisms in the (e,e'p) process were called for. This calculation was, however, based on a shell model spectral function, which has *no* strength in the region of the ridge at large k and E. Therefore the (p,p'N) process as shown in fig.9 could not move any strength into the region $E \geq$100MeV where the experiment of Lourie *et al* observed the excess cross section. One must consider the strength in the region of the ridge and processes involving the Δ in order to produce large strength in the region where experimentally observed.

4.2 Δ-excitation

At the large missing energies of interest to studies of the correlated strength of the spectral function, a second two-step process can give a large contribution: (e,e'N*) followed by $N^* \rightarrow \pi + p$ (see figure 6). The mass and kinetic energy of the undetected pion can simulate large missing energy. As pointed out in section 3 this process is expected to be a lesser problem than (e,e'p) followed by (p,p'N), but it is still a concern.

L/T-separation?

Traditionally, it is thought that processes involving Δ-excitation mainly appear through the transverse component as Δ-excitation is mainly transverse. As a consequence, several groups attempted or proposed L/T-separations.

In inclusive (e,e') L/T-separations have been shown to be efficient in removing the Δ-contribution [24, 25]. For *exclusive* (e,e'p) processes, the gain due to an L/T separation is not obvious, however. For a two-step process, such as (e,e'N*) followed by $N^* \rightarrow p + \pi$, an L/T separation *cannot be done as a matter of principle* as one does not know the kinematics of the primary (e,e'N*) process; the N* is not observed, and the kinematics cannot be reconstructed. If this kinematics is unknown, the separation of the structure functions is not possible. To give one obvious example: The N* can be out-of-plane, while the final observed p is in-plane. The cross section for (e,e'N*) thus involves out-of-plane structure functions one knows nothing about when supposedly doing an in-plane L/T separation.

We also note that L/T-separations in general are a tool of extremely limited dynamical range. As soon as the L- or T-contribution is less than $\sim$ 20% of L+T (as is the case for

the momentum transfers of interest here), the systematic errors of the separation lead to unacceptably large uncertainties on the small component. This is true in particular when one deals with continuum observables. This is well-known from L/T separations of the inclusive (e,e') cross section [25] where, despite extensive efforts, several experiments led to an incorrect Coulomb sumrule. For the coincidence reaction (e,e'p) the experimental accuracy will be worse as (e,e'p) experimentally is significantly more difficult than (e,e').

To estimate the usefulness of L/T separations, and the usefulness of the enhancement of L over T, we have looked at the (e,e'p) experiments performed up to now, by correlating the ratio σ_{IA}/σ_{exp} with the percentage with which the longitudinal cross section in σ_{IA} contributes to the total cross section. If the T-contribution would be the main problem (and if one forgets the fact that L/T separations are not possible for multi-step reactions), one would expect a clear correlation: large $\sigma_L/\sigma_{tot} \leftrightarrow \sigma_{IA}/\sigma_{exp} \approx 1$, and small $\sigma_L/\sigma_{tot} \leftrightarrow \sigma_{IA}/\sigma_{exp} \ll 1$. In this case one could hope that an L/T separation would allow to help suppress the two-step (e,e'N*) + N* $\rightarrow \pi p$ contribution. Fig. 11 shows no such correlation.

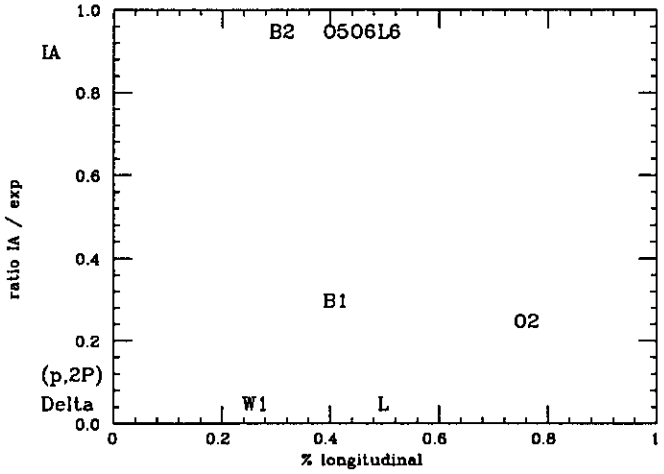

Figure 11: Absence of correlation between relative contribution of longitudinal cross section to σ_{IA} and ratio of σ_{IA} to σ_{exp}, for existing data at large k, E. The vertical scale is accurate to a factor of 2 due to neglected FSI corrections, radiative corrections, *etc.*

For the two reasons given, suppression of T by an L/T separation does not appear to provide an efficient means to suppress two-step contributions involving the Δ. The partly transverse nature of the data available obviously is not the cause for the deviations from IA observed.

Kinematical suppression

The cross section for the process (e,e'N*) followed by N* $\rightarrow \pi p$ is given by the product of the following factors: spectral function $S(k', E')$ of the nucleon hit by the electron, $N \rightarrow N^*$ cross section, angle-dependent cross section of the $N^* \rightarrow \pi p$ process, and kinematical factors of order 1. The $N \rightarrow N^*$ cross section is weakly dependent on kinematics, the main dependence is a decrease as $\mid M_{N^*} - M_\Delta \mid$ increases, the πp cross section has little angular dependence (we ignore factors of 2). The main variable that influences the ratio of two-step to one-step processes thus again is the size of $S(k', E')$. Two-step contributions are expected to be small if the kinematics of the reaction are such as to make $S(k', E')$ as small as possible as compared to the $S(k, E)$ one wants to measure using the one-step (e,e'p) process.

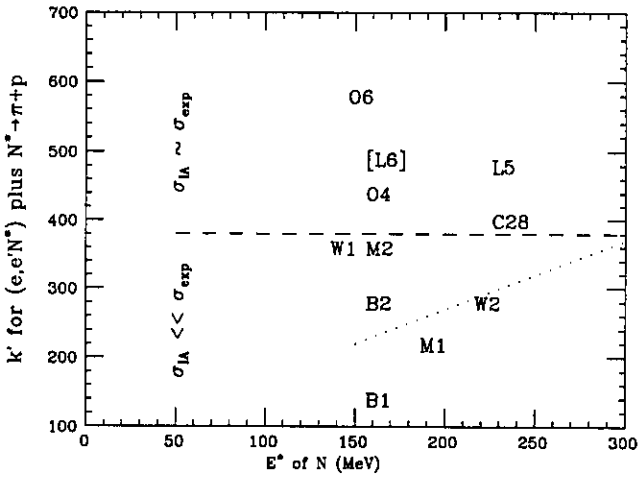

Figure 12: Correlation between k' of initial nucleon hit in (e,e'N*) and ratio σ_{exp}/σ_{IA}. The dashed line separates experiments which give cross sections close (far) from IA.

This question can again be studied by looking primarily at the kinematics. We have, for the various kinematics experimentally explored, studied the range of values k', E' that contribute to the cross section. This has been done by searching for the value of k', E', M_{N^*} and $\theta_{N^* \rightarrow \pi p}$ that best simulate the one-step (e,e'p) kinematics. In figure 12 we show the result. We find that

1) for most kinematics explored the (e,e'p) process for large E can be simulated by (e,e'N*) followed by N* $\rightarrow p\pi$. We also find, not surprisingly, that

2) E' is not the main variable that can be used to influence the results; the two-step process involving the Δ always depends on $S(k', E')$ at *small* E'. We find, lastly, that

3) there is a clear correlation between the size of σ_{exp}/σ_{IA} and the value of $S(k', E')$ as a function of k'. For large k', i.e. small $S(k', E')$, σ_{exp}/σ_{IA} is of order 1, for small k', i.e. large $S(k', E'), \sigma_{exp}/\sigma_{IA} \gg 1$ (see fig.12).

This can be easily understood: at the low E' relevant in connection with the (e,e'N*)+(N* $\rightarrow$ π+p) process, $S(k', E')$ drops rapidly with increasing k' (see figure 3). Kinematics that require a maximal k' for the two-step process minimize its contribution as $S(k', E')$ is small.

5 Approach to measure S at large k, E

The previous figures have shown the regions of k', E' that via two-step processes seriously complicate the (e,e'p) measurement of $S(k, E)$. The empirical evidence for the dominance of the two-step processes in many of the (e,e'p) experiments carried out to date is very strong. The tight correlation between kinematics allowing for two-step contributions and cross sections much larger than predicted by IA (and *vice versa*) clearly shows that these two-step processes are the main cause of problems.

The (p,p'N) process adds strength originating from $E' < E$ *and* $k' > k$. The N* $\rightarrow \pi p$ process adds strength originating from mainly $E' < E$. The minimal contributions of these two-step processes will occur in measurements of $S(k, E)$ at values of k *above* the ridge $k^2/2m = E$.

Depending on the exact kinematics, the locus k', E' from which nucleons that undergo 2-step processes originate has a different shape. The kinematics can be chosen such that this locus covers largely the region where $S(k', E') < S(k, E)$. For the 2-step (p,p'N) reaction the locus of $S(k', E')$ contributing is close to a straight line oriented as in fig.9 for parallel (and antiparallel) kinematics, opening up to a very broad locus for perpendicular kinematics (see fig.13).

(e,e'p) in the region $k < k_{ridge}$ or antiparallel kinematics can be simulated particularly easily with the 2-step reaction (e,e'N*) followed by decay of the N^*. For parallel kinematics and $k > k_{ridge}$ this two-step process can only contribute when the hit nucleon has extremely large k' (i.e. small $S(k', E')$)

The numerical studies also confirm the qualitative insight that kinematics with $\vec{k}$ and $\vec{q}$ close to parallel are the optimal choice when aiming at large k. In parallel kinematics large $\vec{k}$ leads to large $\vec{k}+\vec{q}$, *i.e.* large momentum and energy of the knocked out nucleon. When experimentally requiring such a large momentum of the observed nucleon, one suppresses contributions from two-step processes, which normally lead to a *loss* of momentum and energy. Contributions of two-step processes would have to come from $k' > k$, and there $S(k', E')$ is very small.

In order to extract $S(k, E)$ at large k, E the main consideration must be to rely on data where the kinematics are such that $S(k', E')$ involved in two-step processes is as small as possible. This is the main variable influencing the signal/noise ratio, as $S(k, E)$ is the *only steep function* that occurs in the expression of the cross sections. All other functions are weakly dependent on kinematics.

This consideration has not been included in the choice of the (e,e'p) experiments described above or in previous TJNAF proposals, but is at the base of the kinematics proposed here.

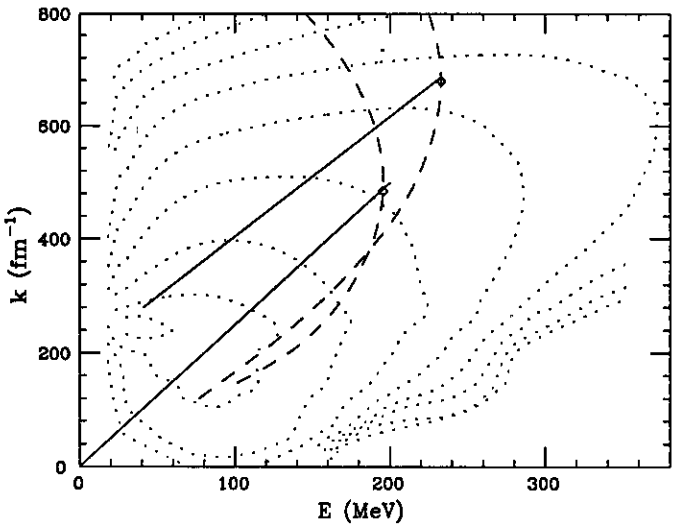

Figure 13: Same as figure 8, but for proposals of Lourie *et al* and Mougey *et al.* In perpendicular kinematics the (p,p'N) process mixes in strength from regions which have a $S(k', E')$ which is much larger than the $S(k, E)$ one tries to measure.

The experiment proposed here involves several features aiming at a separation of the contribution of multistep reactions from the IA strength of $S(k, E)$ at large k and E.

- We chose the kinematics such as to avoid the contribution of multistep reactions as much as possible, in the way discussed in the previous sections.
- We study the cross section as a function of the nuclear mass number A. While the correlated strength is largely independent of the nuclear mass — it essentially directly depends on the N-N interaction — multi-step reactions of the type (e,e'p)+(p,p'N) show a significant dependence on A, as the "target thickness" for the (p,p'N) process is proportional to $A^{1/3}$. We therefore plan to take data on five nuclei between Carbon and very heavy nuclei, spaced by roughly equal increments in $A^{1/3}$.
- We intend to take data on *both sides* of the ridge $E \sim k^2/2m_N$ of the spectral function. While the physics contained in $S(k, E)$ is *the same* the contribution of multistep reactions is much bigger on the large-E/low-k side.
- We intend to take one set of runs in perpendicular kinematics, which, according to figure 13, mixes in multi-step contributions depending on values of k, E where $S(k, E)$ is particularly large.

The latter three points will give us data in situations where the contribution of multi-step reactions gets larger and larger. This will allow to check our calculation of multistep contributions.

In parallel to the experiment proposed, we have started a theoretical program to calculate the contribution of multistep processes. The general idea is to calculate as well as possible these processes, to check the calculation for those kinematics where the two-step contribution is dominant, and then to correct for the two-step contribution in those kinematics where they are small, such as to obtain the spectral function with the smallest theoretical errors possible.

For (e,e'p)+(p,p'N) the theoretical approach developed by us (O. Benhar) is based on
- the momentum and removal energy distribution given by the LDA spectral function calculated as described in ref.[7]
- the SIGCC electron-proton cross section of deForest [26]
- a generalization of Glauber theory suitable to describe the interactions between the recoiling nucleon and the spectator particles, whose spatial distribution is dictated by a realistic many-body wave function including nucleon-nucleon correlations. The approximations implied by this approach, which has been successfully used to describe the FSI in *inclusive* electron scattering [27, 9, 28], are quite accurate for the energies of interest here.
- the parametrized N-N scattering amplitude, of free, or, depending on circumstances, in-medium nucleons.

A similar approach will be used to calculate processes involving pion-production using the available proton data as input.

In order to be able to include additional mechanisms with moderate effort, the Monte-Carlo method is used to simulate the electomagnetic interaction and track the outgoing nucleon through the nucleus. First results for the case of (e,e'p)+(p,p'N) indicate that the computational effort required to predict the multi-step cross section is moderate, and can be handled.

We plan to include the nuclei ^{12}C, ^{27}Al, ^{56}Fe and ^{197}Au. For these nuclei we already have, from the NE3 experiment at SLAC-NPAS [29], a rather comprehensive set of single-arm data at similar energies and angles. These nuclei are evenly spaced in $A^{1/3}$, and are convenient to use experimentally.

We include in our list a fifth nucleus (to be defined) in order to also take data for a nucleus which, under very different kinematics, will be studied in hall A; this will produce for this particular nucleus a more comprehensive data set that will help to further study the reaction mechanism.

We also include in the list of kinematics one setting corresponding to perpendicular kinematics. This type of kinematics is expected to be strongly subject to multistep processes (see figure 13). The region in E_m, p_m covered by the kinematics proposed is displayed in figure 18.

6 Kinematics and time request

6.1 (E_m, p_m) Region of Interest

As has been discussed in section 5 multi-step processes are best suppressed by exploring $S(p_m,E_m)$ in the region of E_m and p_m above the ridge of the spectral function and with kinematics close to "parallel" ones.

The limits of the kinematically accessible E_m, p_m region are determined by the phase space of the experimental facility, i.e. beam energy and detector acceptance, and by the condition of near-parallel kinematics (small angle θ_{qk} between proton initial momentum $\vec{k}(=\vec{p}_m)$ and three-momentum transfer $\vec{q}$). Figure 14 shows the boundaries of the kinematically accessible E_m, p_m regions with an electron beam of energy 1 - 4 GeV, the spectrometers HMS and SOS of Hall C, and three different angles between $\vec{k}$ and $\vec{q}$, θ_{qk} = 10°, 30° and 50°. The region suitable for the measurement of one-step (e,e'p) is above the ridge of the spectral function and below the (E_m, p_m) space boundaries.

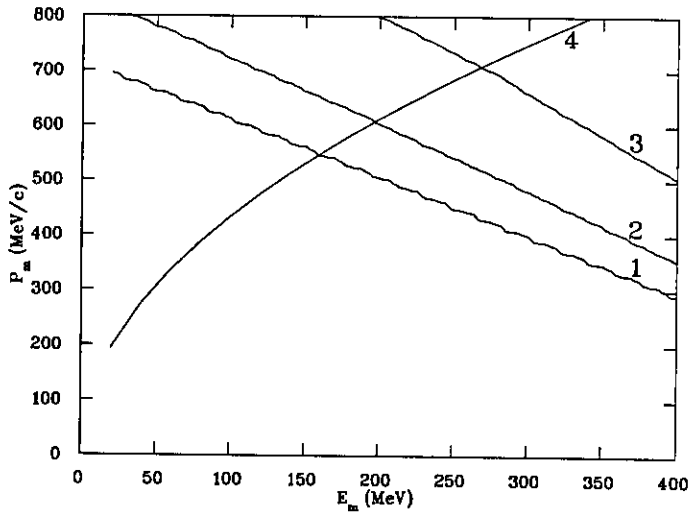

Figure 14: Kinematically accessible range of E_m, p_m. Lines 1 to 3 correspond to angles $\Theta_{kq} = 10°, 30°, 50°$, line 4 represents the ridge of the spectral function.

We have based our simulation on θ_{qk} = 30°, which was chosen as a compromise between large E_m, p_m phase space and close-to-parallel kinematics. The kinematics chosen have been optimized for measurement of the spectral function $S(p_m,E_m)$ at five different locations in the (E_m, p_m) space as shown in the top-left picture of the Figure 15. The corresponding kinematics is listed in the Table 1.

The other five pictures in figure 15 show the phase space of the five kinematics projected onto the (E_m, p_m) plane. The maximum acceptance is placed in the region where the spectral function is small. The sum of the phase space of the five kinematics covers

Table 1: Kinematics

kinematics	1	2	3	4	5
P_m (MeV/c)	750	650	550	450	350
E_m (MeV)	75	75	75	45	35
E_{beam} (GeV)	4.0	3.2	3.2	3.2	2.4
$P_{e'}$ (MeV/c)	1050	1100	1350	1400	1200
$\theta_{e'}(^\circ)$	17.5	16.5	20.0	27.0	31.0
P_p (MeV/c)	3650	2750	2500	2490	1850
$\theta_p(^\circ)$	12.5	13.5	15.5	19.5	28.0

the entire area of interest.

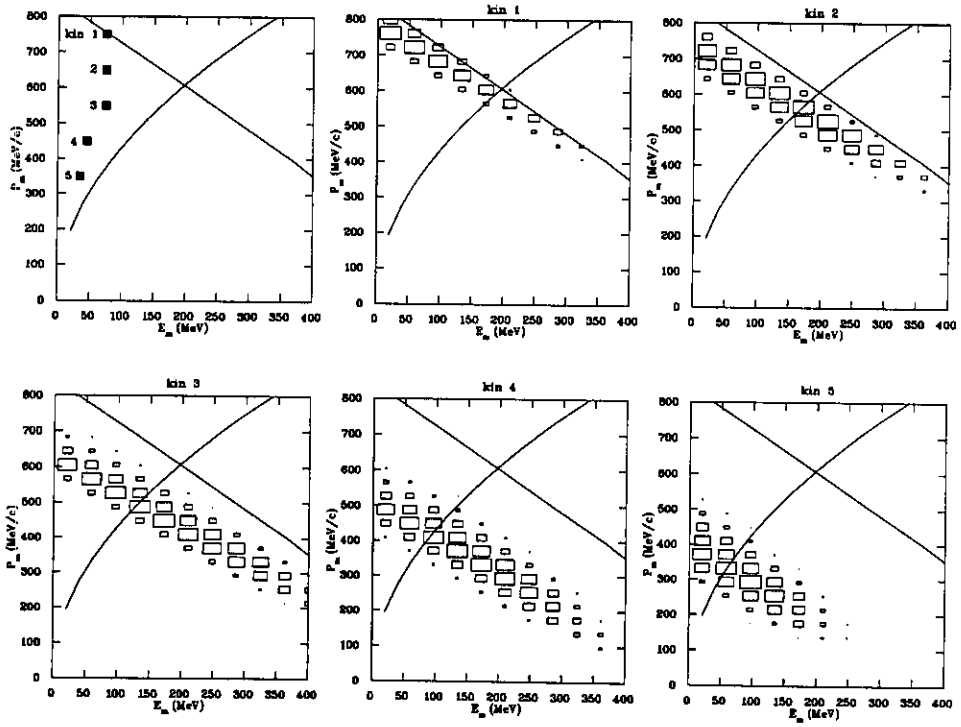

Figure 15: The top left figure shows the optimized settings for the central acceptance. The remaining five plots show the kinematical phase space accepted in the five kinematics chosen. The ridge of the spectral function is indicated by the line.

6.2 Rate estimate

The Monte Carlo calculation has been performed using the simulation code MCEEP[30] which calculates the coincidence (e, e'N) cross section in PWIA. The calculation of the cross sections for singles is based on the routines of Lightbody and O'Connell[31] which include channels of (e, e'), (e, π^-), (e, π^+) and (e, p).

To test the simulation, computations of cross sections have been performed for the kinematics of available (e, e'p) data. Figure 16 shows the comparison between calculation and a ^{3}He(e, e'p) experiment[32]. This calculation was performed using the ^{3}He spectral function [33].

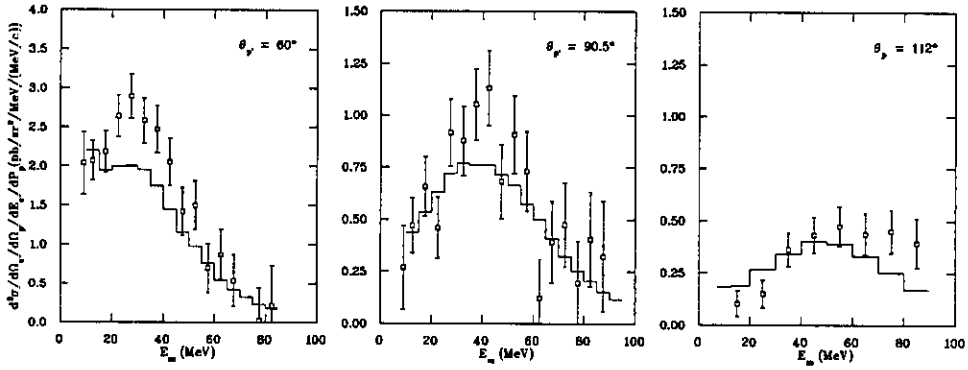

Figure 16: Comparison of calculation and data for $^3He(e,e'p)$, E_e=560MeV, $E_{e'}$=360MeV, $\Theta_{e'}$=25°.

spectrometer	Δ P/P	p_{cent} (MeV/c)	ΔΦ (mrad)	ΔΘ (mrad)
HMS (proton)	±10	4000	55	140
SOS (electron)	±15	1800	115	75

Table 2: Spectrometer specifications

The counting rates for the one-step reaction were calculated for one specific nucleus where the spectral function was available [7], i.e. ^{16}O. For estimates of the rates in the continuum, the particular nucleus used is unimportant. The rates of true coincidences and accidentals for the five kinematics are listed in the appendix, and have been obtained assuming the spectrometer specifications listed in Table 2.

The statistical errors in the spectral function measurement are given by $\delta^{stat}S/S = \delta^{stat}N_{e,e'p}/N_{e,e'p}$, where $N_{e,e'p} = N_{total}$-N_{acci}. N_{total} is the number of count within the coincidence time window, accumulated during the period of run time, and $N_{acci} = N_{acci}^{(e,p)} + f\cdot\sum N_{acci}^{(\pi,x)}$, is the total accidental counts, where f is the inefficiency of the Čerenkov

Table 3: Run parameters

kinematics	1	2	3	4	5
run time(hr)	28	10	2	2	3
luminosity(μA·g/cm^2)	100	20	100	50	50

detectors in pion identification ($\sim$ 0.3% for HMS and SOS) and $N_{acci}^{(\pi,x)}$'s are accidental channels that involve pions. Therefore, δ^{stat}S/S = δ^{stat}(N_{total}-N_{acci})/(N_{total}-N_{acci}) = $\sqrt{N_{total}+N_{acci}}$/($N_{total}$-$N_{acci}$).

The rates leading to tables 5-9 were calculated in PWIA, i.e. without taking into account the absorption of the outgoing nucleon. Averaged over all nuclei, the fraction of nucleons absorbed amounts to $\sim$50%. This additional reduction was incorporated in the estimates for the statistical precision to be achieved. The running times have been adjusted to yield a statistical precision of $\sim$3%.

The systematical errors of the measured cross sections will be dominated by the uncertainty in the knowledge of the overall efficiency ($\pm$2%) resulting from the calibration with the liquid hydrogen, and the contribution due to the uncertainty in the momentum dependence of the spectrometer acceptance, estimated to be $< \pm$2%. Uncertainties due to charge measurement, pion contamination, knowledge of the incident energy *etc* are estimated to be smaller. We thus expect that the overall systematical error in the continuum cross section will be of order 3–4%.

The main systematical error in the determination of the stength of the spectral function at large initial momentum and energy will arise from the *theoretical corrections needed to remove the remaining multi-step processes.* This error at the present time is difficult to quantify. Assuming that, for the optimal kinematics, the contribution of the multistep reactions is below 50% of the (e,e'p) cross section, and assuming that we can calculate the multistep cross section (after "calibration" of the code to cases where multistep processes are the dominant contribution) to $\pm$25%, we can expect to measure $S(k,E)$ at large k, E to $\pm$ 15%. Achieving such an accuracy would be a big step forward in our knowledge of the strength due to correlations.

In oder to calculate the beam times needed, we assumed a target thickness of 1g/cm^2 for the lighter elements, and 0.5g/cm^2 for the heavier ones. For all targets we assumed 100μA as a practical upper limit for the beam intensity. We assume CW beam, and a 1ns coincidence time window.

The running time for the 5 kinematics for one nucleus amounts to 45h on average. In the choice of the luminosity, the condition of $N_{acci}/N_{total} \leq 0.5$ for each (E_m, p_m) bin is employed. The beam time are chosen such that all five kinematics have roughly comparable statistics. The choices of run time and luminosity for the five kinematics are listed in table 3. The results of δ^{stat}S/S, in 40MeV$\times$40MeV/c (E_m, p_m) bins, are shown graphically in Figure 17 and numerically in Table 10 – 12.

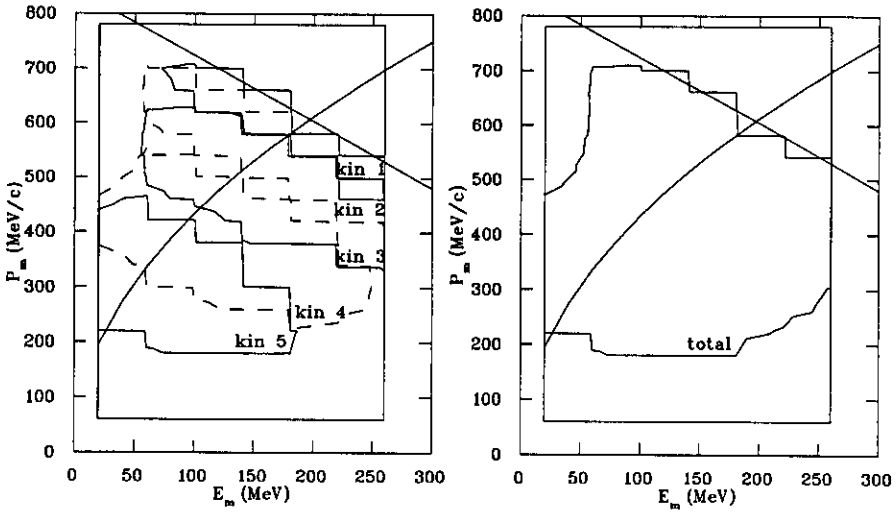

Figure 17: Region in k, E where in the individual kinematics (left) and in the overall data (right) a statistical error of <3% is achieved.

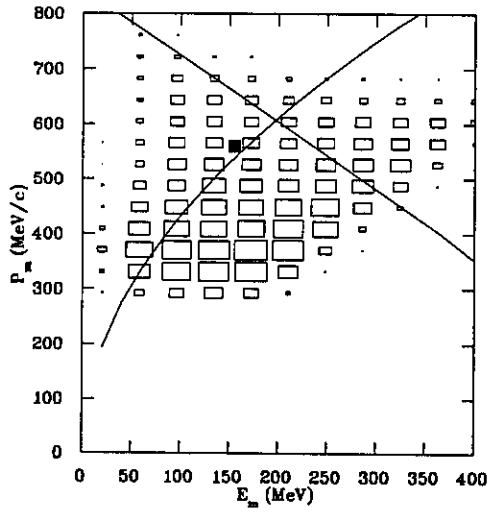

Figure 18: Region of E_m, p_m covered in perpendicular kinematics.

As a reference, the results of the rate calculation using 1ns coincidence time window, 25μA·g·cm^{-2} luminosity and cw electron beam for all five kinematics are shown in Hz and 40MeV×40MeV/c (E_m, p_m) bins in Table 5 - 9. With the calculated rates, scaling the luminosity by a factor of x will result in (e, e'p) and accidental rates being scaled by factors of x and x^2 respectively, while scaling the coincidence time window by a factor of

y results only in scaling the accidental rates by the same factor.

6.3 Beamtime

The beam times needed for the main data taking runs have been discussed above. In table 4 we also include the time needed for a data run in perpendicular kinematics, which we want to take for some of the targets in order to study the multistep-processes. The total amount of time for these runs is estimated to amount to 50h.

In addition we need data on liquid hydrogen to calibrate the efficiencies of the HMS and SOS detector setup. We include 30h total for these calibrations and other checks such as the measurement of the effective acceptance as a function of scattered particle momentum.

In order to have some verification on the radiative correction procedure, we plan to also take, for 2 nuclei, data that allow to check the radiative unfolding. To this end we will include runs at higher SOS energy (400MeV); under the near-parallel kinematics of interest here the radiative effects mainly shift strength in the direction along the axis of the acceptance in E_m, p_m. If practical at the time of the experiment (if compatible with users in halls A, B) we also would like to perform some runs at an electron energy 400MeV lower than the 3.2GeV where most of our data will be taken.

activity	number of targets	time
data for 5 kinematics	5	225 h
data for perp. kin.	2	50 h
data for rad. corr.	2	30 h
calibration	1	15 h
momentum acceptance	1	15 h
Overhead (changes)		20 h
Total		355 h

Table 4: Beam time request

The beamtimes listed in table 4 do not yet include any contingency.

References

[1] V.R. Pandharipande, I. Sick, and P. deWitt Huberts. *Rev. Mod. Phys.*, in print, 1997.

[2] A.E.L. Dieperink, T. de Forest, I. Sick, and R.A. Brandenburg. *Phys. Lett.*, 63B:261, 1976.

[3] H. Meier-Hajduk, C. Hajduk, P.U. Sauer, and W. Theis. *Nucl. Phys.*, A395:332, 1983.

[4] C. Ciofi degli Atti, E. Pace, and G. Salmè. *Phys. Rev*, C21:805, 1980.

[5] O. Benhar, A. Fabrocini, and S. Fantoni. *Nucl. Phys.*, A505:267, 1989.

[6] I. Sick, S. Fantoni, A. Fabrocini, and O. Benhar. *Phys. Lett. B*, 323:267, 1994.

[7] O. Benhar, A.Fabrocini, S. Fantoni, and I. Sick. *Nucl.Phys.*, A579:493, 1994.

[8] C. Ciofi degli Atti and S. Simula. *Phys. Rev.*, C53:1689, 1996.

[9] O. Benhar, A. Fabrocini, S. Fantoni, and I. Sick. *Phys. Lett*, B343:47, 1995.

[10] I. Bobeldijk *et al. Phys. Rev. Lett.*, 73:2684, 1994.

[11] K. I. Blomqvist et al. *Phys. Lett.*, B 344:85, 1995.

[12] J.M. Le Goff. *Université de Paris-Sud Centre d'Orsay*, Ph.D. thesis, 1991.

[13] C. Marchand, , M. Bernheim, P.C. Dunn, A. Gérard, J.M. Laget, A. Magnon, J. Morgenstern, J. Mougey, J. Picard, D. Reffay-Pikeroen, S. Turck-Chieze, P. Vernin, M.K. Brussel, G.P. Capitani, E. De Sanctis, S. Frullani, and F. Garibaldi. *Phys. Rev. Lett.*, 60:1703, 1988.

[14] G. van der Steenhoven, H.P. Blok, M. Thies, and P.J. Mulders. *Phys. Lett.*, 191B:227, 1987.

[15] L.B. Weinstein, H. Baghaei, W. Bertozzi, J.M. Finn, J. Glickman, C.E. Hyde-Wright, N. Kalantar-Nayestanaki, R.W. Lourie, J.A. Nelson, W.W. Sapp, C.P. Sargent, P.E. Ulmer, B.H. Cottman, L. Ghedira, E.J. Winhold, J.R. Calarco, J. Wise, P. Boberg, C.C. Chang, D. Zhang, K. Aniol, M.B. Epstein, D.J. Margaziotis, C. Perdrisat, and V. Punjabi. *Phys. Rev. Lett.*, 64:1646, 1990.

[16] R.W. Lourie, H. Baghaei, W. Bertozzi, K.I. Blomqvist, J.M. Finn, C.E. Hyde-Writht, N. Kalantar-Nayestanaki, J. Nelson, S. Kowalski, C.P. Sargent, W.W. Sapp, P. Ulmer, J. Wiggins, B.H. Cottman, P.K. Teng, E.J. Winhold, M. Yamazaki, J.R. Calarco, F.W. Hersman, J.J. Kelly, and M.E. Schulze. *Phys.Rev.Lett.*, 56:2364, 1986.

[17] P.E. Ulmer, H. Baghaei, W. Bertozzi, K.I. Blomqvist, J.M. Finn, C.E. Hyde-Wright, N. Kalantar-Nayestanaki, S. Kowalski, R.W. Lourie, J. Nelson, W.W. Sapp, C.P. Sargent, L. Weinstein, B.H. Cottman, P.K. Teng, E.J. Winhold, M. Yamazaki Band J.R. Calarco, F.W. Hersman, J.J. Kelly, M.E. Schulze, and G. Audit. *Phys. Rev. Lett.*, 59:2259, 1987.

[18] H. Baghaei, W. Bertozzi, K.I. Blomqvist, J.M. Finn, J. Flanz, C.E. Hyde-Wright, N. Kalantar-Nayestanaki, R.W. Lourie, J. Nelson, W.W. Sapp, C.P. Sargent, P. Ulmer, L. Weinstein, B.H. Cottman, P.K. Teng, E.J. Winhold, M. Yamazaki, J.R. Calarco, F.W. Hersman, C. Perdrisat, V. Punjabi, M. Epstein, and D.J. Margaziotis. *Phys. Rev. C*, 39:177, 1989.

[19] J.H. Morrison. *Ph.D. thesis, MIT*, 1993.

[20] E. Offerman *et al. to be publ.*, 1996.

[21] J. Mougey *et al. CEBAF Proposal*, PR-89-044, 1989.

[22] R. Lourie *et al. CEBAF Proposal*, PR-89-003, 1989.

[23] T. Takaki. *Phys. Rev. Lett.*, 62:395, 1989.

[24] J. Jourdan. *Nucl. Phys. A*, 603:117, 1996.

[25] J. Jourdan. *Phys.Lett.*, B 353:189, 1995.

[26] T. de Forest. *Nucl. Phys.*, 392:232, 1983.

[27] O. Benhar, A.Fabrocini, S. Fantoni, G.A. Miller, V.R. Pandharipande, and I. Sick. *Phys. Rev.*, C44:2328, 1991.

[28] O. Benhar, A. Fabrocini, S. Fantoni, V.R. Pandharipande, S.C. Pieper, and I. Sick. *Phys. Lett. B*, 359:8, 1995.

[29] D. Day, J.S. McCarthy, Z.E. Meziani, R. Minehart, R.M. Sealock, S. Thornton, J. Jourdan, I. Sick, B.W. Filippone, R.D. McKeown, R.G. Milner, D. Potterveld, and Z. Szalata. *Phys.Rev.C*, 40:1011, 1989.

[30] P. Ulmer.

[31] J.W. Lightbody and J.S. O'Connell. Computer in Physics:57, 1988.

[32] C. Marchand. *Thesis, l'Université de Paris-sud Centre d'Orsay*, 1987.

[33] G. Salmé. *priv. com.*

Table 5: Calculated rates(Hz) for kinematics 1 (coincidence window = 1ns; luminosity = 25μA·g·cm^{-2}; cw beam)

$P_{m(MeV)} \backslash E_{m(MeV)}$		20.	60.	100.	140.	180.	220.	260.
^{16}O(e, e'p)	740.	0.001	0.014	0.004				
	700.		0.029	0.067	0.012			
	660.		0.007	0.193	0.487	0.090		
	620.			0.014	0.385	0.294		
	580.				0.046	0.492	0.137	
	540.					0.128	0.408	0.177
	500.						0.029	0.212
$(e', p)_{acci}$	740.	0.013	0.019	0.002				
	700.	0.002	0.014	0.011	0.001			
	660.		0.002	0.015	0.015	0.001		
	620.			0.001	0.009	0.004		
	580.				0.001	0.005	0.001	
	540.					0.001	0.004	0.002
	500.							0.003
$(e', \pi^+)_{acci}$	740.	0.001	0.002					
	700.		0.002	0.001				
	660.			0.002	0.002			
	620.				0.001	0.001		
	580.					0.001		
	540.						0.001	
	500.							
$(\pi^-, p)_{acci}$	740.	0.026	0.030	0.002				
	700.	0.004	0.028	0.017	0.001			
	660.		0.004	0.029	0.023	0.001		
	620.			0.001	0.016	0.006		
	580.				0.002	0.011	0.002	
	540.					0.003	0.008	0.003
	500.						0.001	0.006
$(\pi^-, \pi^+)_{acci}$	740.	0.002	0.003					
	700.	0.001	0.004	0.002				
	660.		0.001	0.005	0.004			
	620.				0.003	0.001		
	580.					0.002		
	540.						0.001	0.001
	500.							0.001

Table 6: Calculated rates(Hz) for kinematics 2 (coincidence window = 1ns; luminosity = 25μA·g·cm^{-2}; cw beam)

$P_{m(MeV)} \backslash E_{m(MeV)}$		20.	60.	100.	140.	180.	220.	260.
^{16}O(e, e'p)	740.	0.009	0.037					
	700.	0.023	0.294	0.258				
	660.	0.028	0.565	2.321	0.875			
	620.	0.004	0.302	3.063	6.429	1.711		
	580.		0.056	1.479	10.317	12.261	1.535	
	540.			0.144	4.258	15.944	11.968	0.117
	500.				0.366	4.610	12.523	4.959
$(e', p)_{acci}$	740.	0.247	0.091					
	700.	0.265	0.261	0.065				
	660.	0.123	0.252	0.306	0.042			
	620.	0.005	0.075	0.256	0.240	0.040		
	580.		0.010	0.088	0.316	0.238	0.026	
	540.			0.007	0.116	0.302	0.228	0.004
	500.				0.009	0.097	0.286	0.162
$(e', \pi^+)_{acci}$	740.	0.020	0.007					
	700.	0.025	0.024	0.006				
	660.	0.011	0.023	0.029	0.004			
	620.		0.007	0.023	0.022	0.004		
	580.		0.001	0.007	0.026	0.020	0.002	
	540.			0.001	0.008	0.023	0.017	
	500.				0.001	0.006	0.020	0.011
$(\pi^-, p)_{acci}$	740.	0.137	0.045					
	700.	0.167	0.150	0.032				
	660.	0.090	0.158	0.160	0.021			
	620.	0.005	0.063	0.155	0.125	0.017		
	580.		0.008	0.069	0.201	0.132	0.013	
	540.			0.006	0.085	0.185	0.117	0.001
	500.				0.008	0.078	0.173	0.083
$(\pi^-, \pi^+)_{acci}$	740.	0.009	0.003					
	700.	0.016	0.013	0.003				
	660.	0.009	0.015	0.015	0.002			
	620.		0.006	0.015	0.012	0.002		
	580.		0.001	0.006	0.018	0.012	0.001	
	540.				0.006	0.015	0.009	
	500.				0.001	0.005	0.012	0.006

Table 7: Calculated rates(Hz) for kinematics 3 (coincidence window = 1ns; luminosity = $25\mu A \cdot g \cdot cm^{-2}$; cw beam)

$P_{m(MeV)} \backslash E_{m(MeV)}$	20.	60.	100.	140.	180.	220.	260.
$^{16}O(e, e'p)$ 700.	0.004	0.006					
660.	0.024	0.171	0.048				
620.	0.062	0.628	0.897	0.160			
580.	0.094	1.405	3.066	3.458	0.276		
540.	0.049	1.604	5.522	8.809	5.267	0.304	
500.	0.003	0.756	5.821	13.805	10.324	2.872	
460.		0.080	2.478	10.243	15.723	7.368	1.248
$(e', p)_{acci}$ 700.	0.048	0.006					
660.	0.129	0.068	0.007				
620.	0.192	0.145	0.063	0.005			
580.	0.164	0.231	0.152	0.080	0.004		
540.	0.046	0.169	0.215	0.172	0.075	0.005	
500.	0.002	0.051	0.175	0.246	0.152	0.047	
460.		0.003	0.054	0.175	0.265	0.148	0.041
$(e', \pi^+)_{acci}$ 700.	0.006	0.001					
660.	0.015	0.008	0.001				
620.	0.020	0.017	0.007	0.001			
580.	0.016	0.023	0.017	0.009			
540.	0.005	0.016	0.021	0.018	0.008	0.001	
500.		0.005	0.016	0.024	0.015	0.005	
460.			0.005	0.016	0.025	0.014	0.004
$(\pi^-, p)_{acci}$ 700.	0.033	0.004					
660.	0.094	0.051	0.005				
620.	0.156	0.117	0.048	0.003			
580.	0.150	0.183	0.124	0.059	0.003		
540.	0.054	0.151	0.175	0.138	0.056	0.003	
500.	0.002	0.060	0.163	0.201	0.124	0.035	
460.		0.004	0.061	0.159	0.222	0.125	0.029
$(\pi^-, \pi^+)_{acci}$ 700.	0.004	0.001					
660.	0.011	0.006	0.001				
620.	0.017	0.014	0.006				
580.	0.015	0.019	0.014	0.007			
540.	0.005	0.015	0.018	0.015	0.006		
500.		0.006	0.015	0.020	0.013	0.004	
460.			0.006	0.015	0.021	0.012	0.003

Table 8: Calculated rates(Hz) for kinematics 4 (coincidence window = 1ns; luminosity = 25μA·g·cm^{-2}; cw beam)

$P_{m(MeV)} \backslash E_{m(MeV)}$		20.	60.	100.	140.	180.	220.	260.
^{16}O(e, e'p)	580.	0.030	0.123					
	540.	0.090	0.540	0.609				
	500.	0.229	1.591	2.317	0.495			
	460.	0.481	3.694	6.062	4.006	0.482		
	420.	0.451	5.544	8.462	8.010	1.973	0.123	
	380.	0.342	4.955	10.810	8.102	3.520	0.622	
	340.	0.024	1.204	5.210	5.601	3.203	1.249	0.144
$(e', p)_{acci}$	580.	0.035	0.014					
	540.	0.054	0.033	0.013				
	500.	0.081	0.056	0.035	0.005			
	460.	0.087	0.077	0.064	0.036	0.005		
	420.	0.039	0.074	0.069	0.068	0.023	0.002	
	380.	0.011	0.038	0.071	0.071	0.046	0.014	
	340.		0.006	0.028	0.048	0.047	0.034	0.009
$(e', \pi^+)_{acci}$	580.	0.006	0.002					
	540.	0.009	0.005	0.002				
	500.	0.013	0.009	0.006	0.001			
	460.	0.014	0.012	0.010	0.006	0.001		
	420.	0.006	0.012	0.011	0.011	0.004		
	380.	0.002	0.006	0.011	0.011	0.007	0.002	
	340.		0.001	0.004	0.007	0.007	0.005	0.001
$(\pi^-, p)_{acci}$	580.	0.028	0.011					
	540.	0.047	0.029	0.012				
	500.	0.076	0.053	0.033	0.005			
	460.	0.090	0.075	0.061	0.032	0.004		
	420.	0.056	0.081	0.068	0.063	0.021	0.002	
	380.	0.020	0.053	0.081	0.074	0.046	0.012	
	340.	0.001	0.011	0.041	0.059	0.052	0.032	0.008
$(\pi^-, \pi^+)_{acci}$	580.	0.005	0.002					
	540.	0.008	0.005	0.002				
	500.	0.012	0.009	0.005	0.001			
	460.	0.014	0.012	0.010	0.005	0.001		
	420.	0.009	0.013	0.011	0.010	0.003		
	380.	0.003	0.008	0.013	0.012	0.007	0.002	
	340.		0.002	0.007	0.009	0.008	0.005	0.001

Table 9: Calculated rates(Hz) for kinematics 5 (coincidence window = 1ns; luminosity = $25\mu A \cdot g \cdot cm^{-2}$; cw beam)

$P_{m(MeV)} \backslash E_{m(MeV)}$		20.	60.	100.	140.	180.	220.	260.
$^{16}O(e, e'p)$	460.	0.113	0.270					
	420.	0.416	1.469	0.387				
	380.	1.734	3.819	1.854	0.198			
	340.	3.245	7.021	5.756	0.737			
	300.	4.627	11.837	8.147	1.845	0.177		
	260.	6.171	9.850	6.433	3.483	0.470		
	220.	0.109	2.963	1.863	1.130	0.293	0.017	
$(e', p)_{acci}$	460.	0.011	0.004					
	420.	0.020	0.011	0.002				
	380.	0.022	0.017	0.007	0.001			
	340.	0.015	0.019	0.018	0.004			
	300.	0.009	0.017	0.018	0.009	0.002		
	260.	0.002	0.007	0.010	0.011	0.004		
	220.		0.001	0.004	0.006	0.004	0.001	
$(e', \pi^+)_{acci}$	460.							
	420.	0.001						
	380.	0.002	0.001	0.001				
	340.	0.002	0.002	0.002	0.001			
	300.	0.001	0.002	0.003	0.001			
	260.		0.001	0.001	0.002	0.001		
	220.			0.001	0.001	0.001		
$(\pi^-, p)_{acci}$	460.	0.021	0.007					
	420.	0.040	0.021	0.003				
	380.	0.051	0.035	0.012	0.002			
	340.	0.039	0.041	0.034	0.007			
	300.	0.032	0.045	0.041	0.016	0.003		
	260.	0.008	0.024	0.027	0.026	0.006		
	220.		0.007	0.014	0.018	0.010	0.002	
$(\pi^-, \pi^+)_{acci}$	460.							
	420.	0.001						
	380.	0.003	0.002	0.001				
	340.	0.005	0.005	0.004	0.001			
	300.	0.004	0.006	0.006	0.002	0.001		
	260.	0.001	0.004	0.004	0.004	0.001		
	220.		0.001	0.002	0.003	0.002		

Table 10: Calculated statistical errors in spectral function measurement $\delta S/S$ (%) (run conditions are described in the text.)

$P_{m(MeV)} \backslash E_{m(MeV)}$	20.	60.	100.	140.	180.	220.	260.
All-kin 740.	39.81	4.32	6.13				
700.	17.20	1.41	0.85	1.98			
660.	12.80	0.99	0.33	0.27	0.65		
620.	14.53	1.10	0.33	0.19	0.28		
580.	8.76	0.96	0.38	0.17	0.14	0.35	
540.	5.76	0.74	0.37	0.21	0.13	0.15	0.44
500.	3.19	0.60	0.31	0.23	0.20	0.16	0.23
460.	1.52	0.41	0.28	0.23	0.22	0.23	0.26
420.	0.95	0.29	0.26	0.25	0.30	0.34	0.41
380.	0.47	0.23	0.21	0.27	0.38	0.47	0.70
340.	0.34	0.22	0.20	0.30	0.45	0.67	1.17
300.	0.28	0.17	0.20	0.33	0.52	0.79	2.14
260.	0.24	0.19	0.23	0.31	0.56	1.08	2.61
220.	1.80	0.34	0.44	0.58	1.05	2.38	7.22
180.		2.47	1.02	0.89	1.91	7.07	20.60
140.					6.37	14.95	114.26

Table 11: Calculated statistical errors in spectral function measurement $\delta S/S$ (%) (run conditions are described in the text.)

$P_{m(MeV)} \backslash E_{m(MeV)}$	20.	60.	100.	140.	180.	220.	260.
kin1 740.	73.91	5.30	6.13				
700.	61.13	2.41	1.08	1.98			
660.		4.01	0.53	0.29	0.65		
620.			1.77	0.32	0.36		
580.				0.91	0.27	0.51	
540.					0.53	0.30	0.46
500.						1.12	0.42
460.							0.93
kin2 740.	32.64	4.10					
700.	15.39	1.45	1.23				
660.	9.99	0.99	0.41	0.63			
620.	15.16	1.26	0.36	0.24	0.46		
580.		2.80	0.51	0.19	0.17	0.48	
540.			1.61	0.29	0.15	0.17	1.77
500.				0.99	0.28	0.17	0.27
460.					1.23	0.32	0.28
420.						1.37	0.63
380.							4.09
kin3 660.	35.34	4.12	5.56				
620.	17.02	1.78	1.10	2.32			
580.	10.57	1.07	0.56	0.49	1.69		
540.	10.94	0.89	0.41	0.30	0.38	1.61	
500.	32.10	1.19	0.38	0.24	0.27	0.52	
460.		3.34	0.57	0.28	0.22	0.33	0.84
420.			4.71	0.51	0.35	0.36	0.53
380.				2.21	0.84	0.53	0.71
340.						1.40	1.31
300.						18.18	4.25

Table 12: Calculated statistical errors in spectral function measurement $\delta S/S$ (%) (run conditions are described in the text.)

$P_{m(MeV)} \backslash E_{m(MeV)}$	20.	60.	100.	140.	180.	220.	260.
kin4 580.	15.47	3.12					
540.	6.65	1.30	1.07				
500.	3.33	0.70	0.53	1.13			
460.	1.82	0.43	0.32	0.40	1.15		
420.	1.54	0.34	0.27	0.28	0.57	2.35	
380.	1.49	0.35	0.24	0.28	0.43	1.07	
340.	5.29	0.71	0.34	0.33	0.45	0.76	2.55
300.		1.69	0.57	0.47	0.56	0.79	2.47
260.			3.12	1.03	0.72	1.08	2.61
220.					2.17	2.59	7.22
180.						15.02	20.60
140.							114.26
kin5 460.	2.79	1.26					
420.	1.22	0.51	0.98				
380.	0.49	0.31	0.45	1.38			
340.	0.34	0.23	0.25	0.71			
300.	0.28	0.17	0.21	0.45	1.52		
260.	0.24	0.19	0.24	0.32	0.91		
220.	1.80	0.34	0.44	0.58	1.20	5.99	
180.		2.47	1.02	0.89	1.91	8.00	
140.					6.37	14.95	